12.2 A mm-Wave/Sub-THz Synthesizer-Free Coherent Receiver with Phase Reconstruction Through Mixed-Signal Kramer-Kronig Processing

Sherif Ghozzy*, Muhamed Allam*, Emir Ali Karahan, Zheng Liu, Kaushik Sengupta

Princeton University, Princeton, NJ *Equally Credited Authors (ECAs)

 $\frac{\mathbf{C}}{\mathbf{S}}$ High frequency wireless systems operating in the high mmWave and sub-THz $\stackrel{\star}{\mathcal{B}}$ frequencies can enable new applications in communication, sensing and imaging, if they Žcan operate with low latency in high resource-constrained environments. In particular, for one-to-many network nodes where the receivers can be highly energy-limited, processing traditional spectrally-efficient signals that utilize both amplitude and phase modulation (e.g., QPSK, 16/64-QAM etc.) places a significant power burden on high-fidelity frequency and phase synthesis, and Tx-to-Rx synchronization at the receiver (Rx) \sum [1,2]. For such coherent communication, the Rx needs to implement its own phase-Slocked loop with integer/fractional frequency synthesis, carrier recovery and synthesis, carrier recovery and synthesis, carrier recovery and synthesis, carrier recovery and synthesis, the strict power and latency requirements for such complex synchronization make many critical low power applications infeasible. Non-coherent communication based on on-off keying alleviates the synchronization issue, but comes with a significant penalty for spectral efficiency. In addition to the burden of frequency synthesis, for directional links, LO distribution (and buffering) to all Rx elements can dissipate significant power (comparable to all elements combined). In this paper, we present a proof-of-concept, synthesizer-free, coherent mmWave/sub-THz Rx architecture that eliminates the need হ্বfor frequency synthesis for coherent demodulation. By optimally designing the Stransmitted spectrum, we enforce an analytical condition on the amplitude and phase functions of the baseband signal. This condition, popularly known as Kramer-Kronig, allows us to estimate the phase of the signal from its amplitude information (via a simple envelope detector) through a Hilbert transform. While this was first proposed in [3] and $\vec{\mathfrak{C}}$ demonstrated recently in optical/THz communication [4,5], the reconstruction was $\widehat{\lnot}$ achieved with dedicated high-speed, power-hungry commercial components and DSPbased Rx, defeating the low-power nature of such Rx. Here, we demonstrate an end-to-end synthesizer-free Rx architecture with low power envelope detection, analog signal processing, and broadband Hilbert N-path FIR filter. With the proposed phase reconstruction scheme, we successfully demonstrate 16-QAM links operating at Gbps. The architecture is translatable to Rx operating close to and beyond fmax.

Analytic signals are complex valued functions that do not have a negative frequency component. Traditional wireless communication signals do not have an analytic relationship, and therefore, their phase information is lost once we pass it through an envelope detector to detect amplitude. An analytical signal $(s_a(t))$ can be constructed from an intended real baseband signal (s(t)) as $s_a(t) = s(t) + j\hat{s}(t)$, where $\hat{s}(t)$ is the Hilbert transform of s(t) i.e. $\hat{s}(t) = H(s(t)) = \frac{1}{\pi} \mathcal{D} \left\{ \int_{-\infty}^{\infty} \frac{s(t)}{t-t} dt \right\}$, and where \mathcal{D} is the Cauchy principal value. This is because the Fourier transform of s(t) and $\hat{s}(t)$ are related as $\mathcal{F}(\hat{s}(t)) = -jsign(\omega)\mathcal{F}(s(t))$ i.e. $\mathcal{F}(s_a(t)) = s(t) + j\hat{s}(t)$ has no negative frequency components. The intuition in creating the analytical condition in the baseband signal is to consider the real up-converted signal $s_{fo}(t) = \mathcal{R}e\{s_a(t)e^{i\omega_0t}\}$ that shows singlesidebanded (SSB) behavior (Fig. 12.2.1). In other words, SSB signals, when frequency down-converted, can allow analytic formulation if certain conditions are satisfied.

Since the resource constrained Rx does not deploy a carrier signal, we deploy the access point transmitter to send the carrier at the edge of the SSB signal ($\mathcal{R}e\{Ae^{i\omega_0t}\}$), as shown in Fig. 12.2.1. This serves two purposes. First, it allows frequency down-conversion at the Rx to a baseband SSB signal via an envelope detection without sacrificing spectral efficiency (Fig. 12.2.1). Secondly, it allows the realization of the analytic condition when the combination signal $s_{Tx}(t) = \mathcal{R}e\{(s_a(t) + A)e^{i\omega_0t}\} = \mathcal{R}e\{|s_{env}(t)|e^{i\phi_0t}e^{i\omega_0t}\}$ passes through the Rx chain. To be precise, the baseband signal $\log(s_{env}(t)) = \log(|s_{env}(t)|) + j\phi(t)$ can be shown to be analytic if the constellation of the signal $(s_{env}(t))$ does not pass through the zero crossing (i.e. $A > |s_a(t)|$) (Fig. 12.2.2). This implies that with a SSB signal and a suitably placed strong carrier at the band-edge, the amplitude signal $\log(|s_{env}(t)|)$ and phase $\phi(t)$ satisfy the Kramer-Kronig relationship. $\phi(t)$ can then simply be obtained through a Hilbert transform of the logarithm of the detected amplitude, allowing full reconstruction of I, Q signals as shown in Fig. 12.2.2. For coherent sub-THz receivers, this can eliminate frequency synthesis, carrier recovery/synchronization, frequency translation and phase alignment in favor of a simple amplitude detection, and efficient mixed-signal blocks performing Hilbert transform.

Figure 12.2.1, shows the implemented architecture. As can be seen, the incident sub-THz signal is amplified through a chain consisting of LNA, envelope detector and square-root module to extract the amplitude. While the envelope detector (square-block) corrupts the baseband spectrum due to the spectral spreading of $|s_{env}(t)|^2$, the phase reconstruction path through the logarithmic amplifier and a broadband Hilbert transform allows us to reconstruct the original I, Q signals.

Figure 12.2.2. shows minimum phase (MP) condition and the simulated reconstructed constellation of such a Rx operating at 100GHz with 1GHz bandwidth, demonstrating superior phase recovery achieved with the proposed signal processing scheme. It can be noted that the Hilbert transform block needs to process baseband signals (near DC to few GHz) with flat group delays, and therefore, cannot be implemented with pure phase shifters commonly employed in narrowband image-rejection receivers. While the ideal Hilbert transform will need an infinite order filter, in this implementation, we choose a 12th- order mixed-signal FIR filter realized with a differential 6-taps N-path filter (Fig. 12.2.3). To process a BW of 2GHz, we time-interleave the sampling with 250ps delays across the 12 taps (generated with a non-overlapping clock generator), effectively employing a sampling rate of 4GHz (Fig. 12.2.3). As shown in the figure, the unit delay steps of the FIR filter are implemented with phase-shifted timing control of the switches. We size the N-path capacitors to realize the Hilbert FIR coefficients, and the switches to allow settling time within 250ps. The filter dissipates only 3.2mW of dynamic power. The LNA is realized as a 4-stage differential design with neutralization and with an onchip balun. The LNA has a simulated gain of 17.3dB, NF of 7.4dB and a bandwidth of 20GHz. The LNA is the highest power dissipating element consuming 36mW of power, and can be even eliminated for beyond-f_{max} coherent Rxs. The figure also shows the broadband square-root and logarithmic amplifier blocks, designed with asymmetrical differential topologies, and with 2GHz of bandwidth.

Figure 12.2.4 shows the measured LNA performance and the square-root and log amplifier. The LNA peaks at 90GHz with a gain of 13dB and a bandwidth of 17GHz. The figure also shows the measured Hilbert transfer function across 100MHz-to-2GHz. While there is a mismatch in certain regions of the transfer function filter, it does not impede phase reconstruction. Figure 12.2.5 shows the measured reconstructed constellations and spectrum at 90, 95 and 100GHz operating at 1Gbps. As can be seen, without any frequency synthesis, the Rx path is able to recover the amplitude and phase signals, successfully reconstructing the high-speed signals. The entire Rx consumes between 36-to-54 mW of DC power. The figure shows the measured EVM against carrier to signal power ratio (CSPR), demonstrating failure of phase reconstruction path, when the Kramer-Kronig relationship does not hold for low CSPR. Due to the nonlinear nature of the processing, the sensitivity is measured directly with EVM data, demonstrating processing capability of -47dBm input signal, at CSPR of 7dB, carrier power of -47.7dBm and QAM signal power of -54.8dBm, when the output EVM increases to -16dB. The table of comparison with state-of-the-art mmWave Rx is shown in Fig. 12.2.6. As can be seen, by enforcing analytical baseband condition through SSB modulation and carrier positioning, the Rx eliminates the need for high-frequency synthesis, synchronization, phase control, and LO distribution, allowing low-power PLL-free mmWave/sub-THz Rx operating with complex modulations with on-chip amplitude detection and phase reconstruction.

Acknowledgement:

The authors would like to thank the Office of Naval Research, the Air Force Office of Scientific Research, the MURI Program, and the DURIP program for funding support. Authors also would like to thank Bert Harrop for professional assistance with packaging.

References:

- [1] M. I. Ibrahim et al., "THzID: A 1.6mm2 Package-Less Cryptographic Identification Tag with Backscattering and Beam-Steering at 260GHz," *ISSCC*, pp. 454-455, Feb. 2020. [2] Suresh. Venkatesh et al., "A high-speed programmable and scalable terahertz holographic metasurface based on tiled CMOS chips." *Nature electronics*, vol. 3, no. 12, pp. 785-793, 2020.
- [3] H. Voelcker, "Demodulation of single-sideband signals via envelope detection," *IEEE Trans. Commun. Technol.* 14, pp.22–30, 1966.
- [4] A. Mecozzi, A. Cristian, and S. Mark, "Kramers-Kronig coherent receiver." *Optica*, vol. 3, no.11, pp. 1220-1227, 2016.
- [5] T. Harter et al., "Generalized Kramers-Kronig receiver for coherent terahertz communications." *Nature Photonics*, vol. 14, nol. 10, pp. 601-606, 2020.

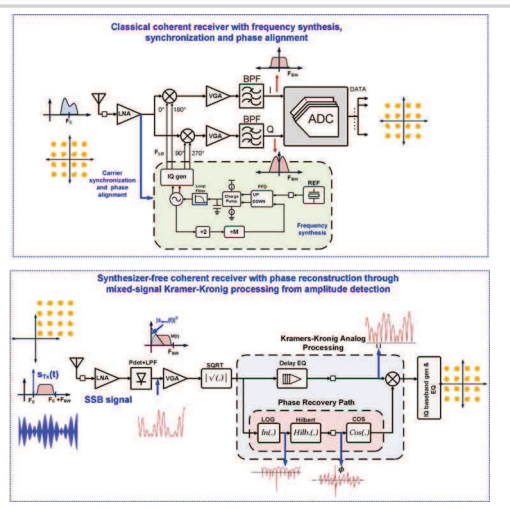
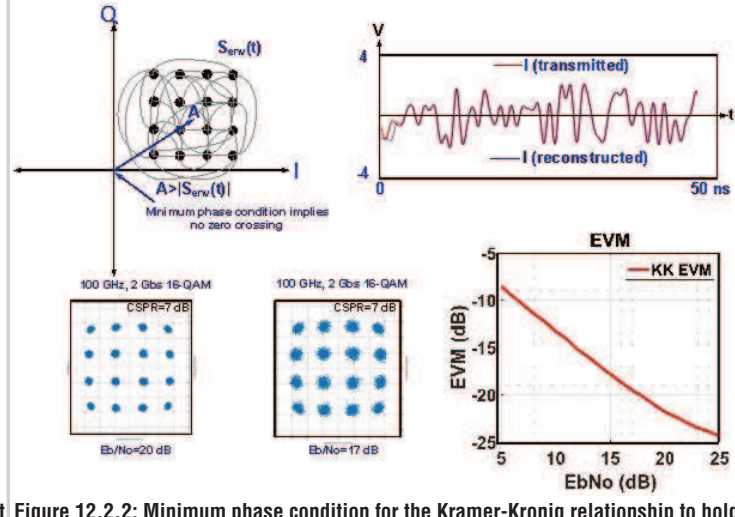


Figure 12.2.1: Principle of operation of the presented synthesizer-free coherent Figure 12.2.2: Minimum phase condition for the Kramer-Kronig relationship to hold mmWave/sub-THz receiver that extracts phase information from the amplitude to allow phase estimation from the amplitude detection. The figure shows simulated detection utilizing the Kramer-Kronig relationship. This is achieved by enforcing reconstructed I signal, and constellation with a 100GHz signal, and 1GHz 16-QAM analytic condition on the baseband signal through SSB modulation with an optimized modulated baseband signal for Eb/No=15 and 20dB. The figure also shows effect of carrier positioning from the transmitter.



EVM against Eb/No for the proposed receiver.

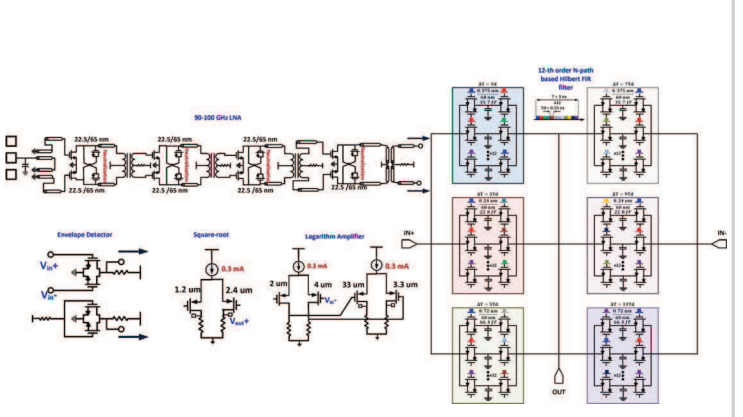
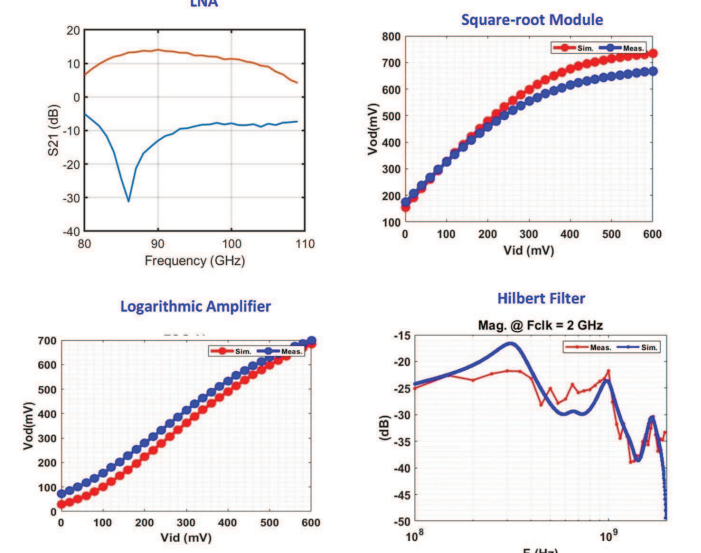


Figure 12.2.3: Schematics of the mmWave and analog circuit blocks including LNA, envelope detector, square-root and logarithmic amplifier. The figure also shows the broadband Hilbert filter realized with a 12th order mixed-signal FIR filtering realized Figure 12.2.4: Measured circuit performances including LNA, square-root and with a N-path filter.



logarithmic amplifier and N-path Hilbert filter.

90 GHz 16-QAM @ 1 Gbps	Reconstructed Spectrum
	Constitution of the Consti
95 GHz 16-QAM @ 1 Gbps	Reconstructed Spectrum
1	Lipros
100 GHz 16-QAM @ 1 Gbps	Reconstructed Spectrum
15	20 - 20 - 20 - 20 - 20 - 20 - 20 - 20 -
EVM VS CSPR	EVM VS Pin
-16	Sensitivity levels of -47 dBm (for -20 dB SNR)
(B) WA 20	(B) -20
.22 .24	22 23 24
4 6 8 10 12 14 16 CSPR (dB)	-24 -50 -45 -40 -35 -30 -25 -20 Pin(dBm)

Figure 12.2.5: Measured reconstructed constellation of the receiver with 90, 95 and 100GHz 16-QAM links operating at 1Gbps. The figure also shows EVM variation with the carrier power, and input power at 90GHz.

	This work	Dong, et.al. JSSC'21	Deng et. al., JSSC'20	Chou et.al., ESSCIRC'22	E. Naviasky, et.al., ISSCC'21	Harter, et al., Nature Photonics 2020
Receiver Architecture	Kramer-Kronig based Coherent receiver	PLL-based MSK receiver	I/Q mixer based receiver	I/Q mixer based receiver (4- element)	I/Q mixer-based (16-element)	Kramer-Kronig based
Process	65nm CMOS	65 nm CMOS	65 nm CMOS	28 nm CMOS	28 nm CMOS	Commercial Waveguide-based LNA+Schottky diode+ DSP
Operating Frequency	90-100 GHz	180 GHz	60 GHz	135 GHz	71-76	300 GHz
Modulation	Coherent (16-QAM)	MSK receiver	QPSK	QPSK/16QAM	QPSK/16-QAM	QPSK/16-QAM
Frequency synthesizer	Not required	On-chip PLL	On-chip PLL	On-chip PLL	On-chip PLL	Commercial signa generator
PLL+ LO Buffer Power consumption	N/A	*	84 mW	152 mW (total)	*	
Data rates	1 Gbps	6-12 Gbps	10 Gbps	12 Gbps	2 Gbps	115 Gbps
IF (3-dB bandwidth)	2 GHz	2	2		2	
Sensitivity	-47 dBm (2 GHz BW, 20 dB SNR)	-32 to -13*	7.1 dB (NF)		9-11 dB (NF)	-33 dBm
Power consumption	36-54 mW LNA: 30-48 mW Rest of Rx: 6 mW (power consumption scales proportionately with number of elements)	126-160 mW	146 mW	98 mW/Rx element+PLL+LO Buffering	1710 mW (total Rx power) 107 mW/Ant	*

Figure 12.2.6: Table of comparison with state-of-the-art mmWave receivers.

ISSCC 2024 PAPER CONTINUATIONS

